NASA TECHNICAL NOTE

NASA TN D-5984

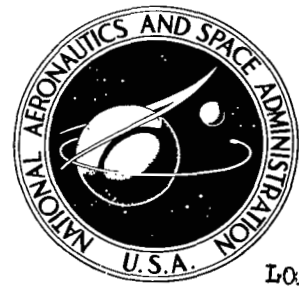

THEORETICAL PRESSURE DISTRIBUTIONS OVER ARBITRARILY SHAPED PERIODIC WAVES IN SUBSONIC COMPRESSIBLE FLOW AND COMPARISON WITH EXPERIMENT

by K. R. Czarnecki and Mary W. Jackson

Langley Research Center
Hampton, Va. 23365

NATIONAL AERONAUTICS AND SPACE ADMINISTRATION • WASHINGTON, D. C. • NOVEMBER 1970

1. Report No.	2. Government Accession No.	3. Recipient's Catalog No.
NASA TN D-5984		

4. Title and Subtitle	5. Report Date
THEORETICAL PRESSURE DISTRIBUTIONS OVER ARBITRARILY SHAPED PERIODIC WAVES IN SUBSONIC COMPRESSIBLE FLOW AND COMPARISON WITH EXPERIMENT	November 1970
	6. Performing Organization Code

7. Author(s)	8. Performing Organization Report No.
K. R. Czarnecki and Mary W. Jackson	L-7124
	10. Work Unit No.
9. Performing Organization Name and Address	126-13-10-12
NASA Langley Research Center Hampton, Va. 23365	11. Contract or Grant No.
	13. Type of Report and Period Covered
12. Sponsoring Agency Name and Address	Technical Note
National Aeronautics and Space Administration Washington, D.C. 20546	14. Sponsoring Agency Code

15. Supplementary Notes

16. Abstract

The theoretical solution for the pressure distribution over an infinitely repeating set of sinusoidal waves in subsonic, compressible flow is extended to the area of arbitrarily shaped, periodic waves by the use of Fourier series, and a simplified or approximate solution for the calculation of first-order effects is developed. The solutions are compared with experimental pressure distributions determined at Mach numbers of 0.70 and 0.90 on six types of finitely repeating roughness elements incorporated into the cylindrical portions of a group of ogive cylinders. Discrepancies between theory and experiment are discussed in detail.

17. Key Words (Suggested by Author(s))	18. Distribution Statement
Theoretical pressure distributions Surface roughness Fourier series approach	Unclassified – Unlimited

19. Security Classif. (of this report)	20. Security Classif. (of this page)	21. No. of Pages	22. Price*
Unclassified	Unclassified	33	$3.00

*For sale by the Clearinghouse for Federal Scientific and Technical Information
Springfield, Virginia 22151

THEORETICAL PRESSURE DISTRIBUTIONS OVER ARBITRARILY SHAPED PERIODIC WAVES IN SUBSONIC COMPRESSIBLE FLOW AND COMPARISON WITH EXPERIMENT

By K. R. Czarnecki and Mary W. Jackson
Langley Research Center

SUMMARY

The theoretical solution for the pressure distribution over an infinitely repeating set of sinusoidal waves in subsonic, compressible flow is extended to the case of arbitrarily shaped, periodic waves by the use of Fourier series, and a simplified or approximate solution for the calculation of first-order effects is developed. The solutions are compared with the experimental pressure distributions of NASA TN D-3516 determined at Mach numbers of 0.70 and 0.90 on six types of roughness elements incorporated into the cylindrical portions of a group of ogive cylinders. The comparisons are discussed in terms of violations of the restrictions and assumptions inherent in the theory. They lead to the following conclusions.

The basic theory has an excellent potential for prediction of inviscid roughness pressure distributions over arbitrarily shaped, periodic surface roughness elements but a smoothing procedure must be incorporated to realize the full potential. For estimation of first-order effects, the approximate or simplified theory is quite satisfactory for approximately sinusoidal shapes, but tends to deteriorate in usefulness as a square-cornered, rectangular roughness shape is approached. Agreement of theory with experiment is poor because boundary-layer effects strongly delay the onset of the compressibility effects predicted by the theory and even prevent the incompressible-flow pressure distribution from being realized. Extension of the theory to predict first-order sweep effects may be possible by using an approach which utilizes the component of the free-stream flow normal to the roughness element.

INTRODUCTION

One of the major obstacles to the attainment of the ultimate theoretical performance of aircraft, either subsonic or supersonic, is the existence of surface roughness drag. This drag is always present to a degree, but theoretically can be reduced to tolerable levels by the construction, at rapidly rising cost, of smoother surfaces held to closer design tolerances. Unfortunately, knowledge about the physical mechanism which induces

the drag is so meager that generally neither the magnitude of the drag nor methods for its reduction can be established with sufficient accuracy to be truly useful. Recent investigations have shown, however, that roughness drag is primarily pressure drag even at subsonic speeds. (See refs. 1 and 2, for example.) This knowledge thus suggests that the first logical step to gain an understanding of the mechanism is to compare theoretical inviscid-flow pressure distributions over relatively simple roughness shapes with experimental distributions to determine the deviations that must be accounted for. This was done in references 3 and 4 for the supersonic flow regime where inviscid wave drag is the main contributor to the drag. Little has been done in subsonic flow where the roughness drag is smaller and the mechanism more obscure, principally because a suitable subsonic theory for pressure distribution has not been available.

The basic objectives of this investigation were twofold. The first was to extend an available solution for subsonic flow over an infinite cylinder of sinusoidal waves to apply to any arbitrarily shaped train of repeating waves. The second was to compare the theory with experiment and to evaluate possible sources for deviations in agreement. Experimental pressure distributions for subsonic flow from reference 4 were used to make the analysis.

SYMBOLS

a,b	coefficients in expansion of a function in a Fourier series
A,B,C,D	arbitrary constants in general solution of basic partial differential equation
C_p	pressure coefficient, $\frac{p_l - p_\infty}{q_\infty}$
h	local roughness coordinate or height in radial direction, measured from mean cylinder radius
$I_0(\mu), K_0(\mu)$	modified Bessel functions of zero order
$K_1(\mu)$	modified Bessel function of first order
l	length of one-half cycle of repeating surface waves
L	length of model
M	Mach number

n integer

p static pressure

q dynamic pressure

r local cylinder radius, measured normal to cylinder axis

R unit Reynolds number (based on a length of 1 meter)

u perturbation velocity in axial direction

U free-stream velocity

v perturbation velocity in radial direction

x axial distance, measured from chosen origin for theory and measured from model nose for experimental data

$\beta = \sqrt{1 - M_\infty^2}$

μ arbitrary function, equal to $\beta n \pi \frac{r}{l}$ in this report

φ perturbation velocity potential

Subscripts:

1,2,3, . . .,n index numbers

l local surface

m mean

max maximum

t total

∞ free stream

THEORY

The basic problem is to determine the theoretical pressure distributions over an infinite cylinder of arbitrarily shaped, periodic transverse waves in a subsonic axisymmetric free-stream flow as depicted in figure 1. The surface of the cylinder is defined by

$$r = r_m + h(x) \tag{1}$$

where the roughness distribution $h(x)$ is cyclic in nature, is an arbitrary function of x within the limits of 1 wavelength ($0 \leqq x \leqq l$), and is measured from the mean cylinder radius r_m. Because the free-stream velocity is dependent upon r_m, the compatability requirement exists that

$$\frac{1}{2l}\int_0^{2l}\left\{\left[h(x) + r_m\right]^2 - r_m^2\right\} dx = 0 \tag{2}$$

If the further restrictions are applied that

$$\left.\begin{aligned} &|h(x)| \ll r_m \\ &\left|\frac{\partial}{\partial x}\left[h(x)\right]\right| \ll 1 \end{aligned}\right\} \tag{3}$$

then the governing partial differential equation for the perturbation velocity potential $\varphi(x,r)$ becomes, in cylindrical coordinates,

$$\beta^2\frac{\partial^2\varphi}{\partial x^2} + \frac{\partial^2\varphi}{\partial r^2} + \frac{1}{r}\frac{\partial\varphi}{\partial r} = 0 \tag{4}$$

where

$$\beta = \sqrt{1 - M_\infty^2}$$

and the perturbation velocity components are found from

$$\left.\begin{aligned} u &= \frac{\partial\varphi}{\partial x} \\ v &= \frac{\partial\varphi}{\partial r} \end{aligned}\right\} \tag{5}$$

Application of these restrictions means, of course, that the theory will not apply to wave shapes which incorporate steps or any other shapes which are expected to have a

stagnation line in inviscid flow. Because of the desire to incorporate β with r rather than x, the general solution of equation (4) appropriate to the present problem is found from the requirement that the velocity components u and v vary monotonically with r. The solution is (for example, see ref. 5, pp. 216-223, or ref. 6, ch. 9):

$$\varphi(x,r) = \sum_{n=1}^{\infty} \left[A_n \cos\left(n\pi \frac{x}{l}\right) + B_n \sin\left(n\pi \frac{x}{l}\right) \right] \left[C_n I_0\left(\beta n\pi \frac{r}{l}\right) + D_n K_0\left(\beta n\pi \frac{r}{l}\right) \right] \tag{6}$$

where I_0 and K_0 are modified Bessel functions of order zero and A_n, B_n, C_n, and D_n are arbitrary constants to be determined for the particular solution.

Examination of equation (6) suggests the possibility of useful developments if, in order to find a particular solution, the roughness distribution is expressed in a Fourier series:

$$h(x) = \sum_{n=1}^{\infty} \left[a_n \cos\left(n\pi \frac{x}{l}\right) + b_n \sin\left(n\pi \frac{x}{l}\right) \right] \tag{7}$$

where

$$\left.\begin{aligned} a_n &= \frac{1}{l} \int_0^{2l} h(x) \cos\left(n\pi \frac{x}{l}\right) dx \\ b_n &= \frac{1}{l} \int_0^{2l} h(x) \sin\left(n\pi \frac{x}{l}\right) dx \end{aligned}\right\} \tag{8}$$

Only two boundary conditions can be specified for the determination of the particular solution but they are sufficient to evaluate the set of four arbitrary constants. These boundary conditions are as follows:

$$\left.\begin{aligned} &u(x,\infty) = 0 \\ \text{or} \quad &\\ &\frac{\partial}{\partial x}\left[\varphi(x,\infty)\right] = 0 \end{aligned}\right\} \tag{9}$$

and, approximately,

$$\left.\begin{aligned} &\frac{v(x,r_m)}{U} \approx \left(\frac{dr}{dx}\right)_l \\ \text{or} \quad &\\ &\frac{\partial}{\partial r}\left[\varphi(x,r_m)\right] = U \frac{\partial}{\partial x}\left[r_m + h(x)\right] = U \frac{\partial}{\partial x}\left[h(x)\right] \end{aligned}\right\} \tag{10}$$

The second boundary condition (eq. (10)) is predicated on the fact that the governing differential equation is linear and thus it is permissible to satisfy the matching of the local velocity with the local surface slope at r_m rather than directly on the surface itself. The first boundary condition (eq. (9)) requires that all constants C_n be zero. This result makes it possible for the constants D_n to be coupled with the constants A_n and B_n to form new constants A_n' and B_n', which can readily be evaluated from the second boundary condition at $x = l$ and $x = \frac{l}{2}$ as follows:

$$\left.\begin{aligned} A_n' &= A_n D_n = -\frac{U}{\beta} \frac{b_n}{K_1\left(\beta n\pi \frac{r_m}{l}\right)} \\ B_n' &= B_n D_n = \frac{U}{\beta} \frac{a_n}{K_1\left(\beta n\pi \frac{r_m}{l}\right)} \end{aligned}\right\} \tag{11}$$

Substitution of these results (eqs. (11)) into equation (6) yields the particular solution for the perturbation velocity potential:

$$\varphi(x,r) = \frac{U}{\beta} \sum_{n=1}^{\infty} \left[a_n \sin\left(n\pi \frac{x}{l}\right) - b_n \cos\left(n\pi \frac{x}{l}\right) \right] \frac{K_0\left(\beta n\pi \frac{r_m}{l}\right)}{K_1\left(\beta n\pi \frac{r_m}{l}\right)} \tag{12}$$

The pressure distributions over the waves are found from

$$C_p\left(x, r_m\right) = -\frac{2}{U} \frac{\partial}{\partial x} \left[\varphi\left(x, r_m\right) \right] \tag{13}$$

which incorporates the usual limitations of linearized theory and the requirement that $r >> |h|$. Equation (13) then becomes

$$C_p\left(x, r_m\right) = -\frac{2}{\beta} \frac{\pi}{l} \sum_{n=1}^{\infty} n \left[a_n \cos\left(n\pi \frac{x}{l}\right) + b_n \sin\left(n\pi \frac{x}{l}\right) \right] \frac{K_0\left(\beta n\pi \frac{r_m}{l}\right)}{K_1\left(\beta n\pi \frac{r_m}{l}\right)} \tag{14}$$

If the cylinder is very slender, so that the ratio of $\frac{r_m}{l}$ is very small, the following asymptotic forms of the Bessel function can be used appropriately (for example, see ref. 6, p. 151):

$$\left.\begin{aligned} K_0(\mu) &\sim -\log_e \mu \\ K_1(\mu) &\sim \mu^{-1} \end{aligned}\right\} \tag{15}$$

The surface pressure coefficient then becomes, approximately,

$$C_p(x, r_m) \approx 2\pi^2 \frac{r_m}{l^2} \sum_{n=1}^{\infty} n^2 \left[a_n \cos\left(n\pi \frac{x}{l}\right) + b_n \sin\left(n\pi \frac{x}{l}\right) \right] \log_e \left(\beta n\pi \frac{r_m}{l}\right) \tag{16}$$

It should be noted, however, that the more appropriate form for the pressure coefficient for very slender bodies in axisymmetric flow is (ref. 7, p. 78)

$$C_p(x, r) = -\frac{2}{U} \frac{\partial}{\partial x} \left[\varphi(x, r)\right] - \frac{1}{U^2} \left\{ \frac{\partial}{\partial r} \left[\varphi(x, r)\right] \right\}^2$$

where the second term on the right can readily be found with use of equation (12).

At the other extreme, when the ratio $\frac{r_m}{l}$ is very large, the appropriate asymptotic forms of the Bessel function are

$$\left.\begin{aligned} K_0(\mu) &\sim \sqrt{\frac{\pi}{2\mu}}\, e^{-\mu} \\ K_1(\mu) &\sim \sqrt{\frac{\pi}{2\mu}}\, e^{-\mu} \end{aligned}\right\} \tag{17}$$

and the surface pressure coefficient is given by

$$C_p(x) \approx -\frac{2\pi}{\beta l} \sum_{n=1}^{\infty} n \left[a_n \cos\left(n\pi \frac{x}{l}\right) + b_n \sin\left(n\pi \frac{x}{l}\right) \right] \tag{18}$$

Equation (18) corresponds to the purely two-dimensional flow case.

The use of equations (14), (16), and (18) allows the pressure distribution to be calculated for any shaped surface of identically repeating waves. The simplest cases occur when the surface waves are sinusoidal or cosinusoidal. When they are sinusoidal, all Fourier coefficients vanish except the b_1 term, which becomes

$$b_1 = h_{max} \tag{19}$$

and equation (14), for example, reduces to

$$C_p\left(x, r_m\right) = -\frac{2\pi}{\beta} \frac{h_{max}}{l} \sin\left(n\pi \frac{x}{l}\right) \frac{K_0\left(\beta\pi \frac{r_m}{l}\right)}{K_1\left(\beta\pi \frac{r_m}{l}\right)} \tag{20}$$

Equation (20) is the solution to the classical sinusoidal wave problem as usually presented in the literature. (See, typically, refs. 7 and 8.) The results for the cosine surface are similar. In general, however, the Fourier series representation of an arbitrarily shaped wave profile requires a considerably larger number of terms in the summation, and the pressure distribution calculations can become rather lengthy. For such cases, one may often desire to be able to make a relatively quick calculation of the pressure distribution without incurring undue losses in accuracy. The possibility of developing such a procedure is examined next.

An analysis of the Fourier coefficients when the formal restrictions of the inequalities (3) are met indicates that the coefficients tend to decrease in magnitude as follows (see ref. 9, p. 127):

$$\left.\begin{aligned} a_n &\propto \frac{1}{n^3} \\ b_n &\propto \frac{1}{n^3} \end{aligned}\right\} \tag{21}$$

This result indicates that the first terms in the summations (the fundamental sine and cosine waves) are by far the most significant contributors to the pressure distribution coefficients and that the higher order terms can possibly be dropped with only a reasonable decrease in accuracy. Furthermore, if the cosine term is suppressed and the surface roughness shape is fitted by a single mean sine wave, as illustrated in figure 2, the influence of one wave on the others in the train will be relatively unaltered. The pressure distribution on a single wave (in an infinite train) is, of course, the result of the sum of the influences of all waves on each other at subsonic speeds. The requirement for the mean fit is

$$h_m = \frac{\int_0^{2l} |h(x)|\, dx}{\int_0^{2l} \left|\sin\left(\pi \frac{x}{l}\right)\right| dx} \tag{22}$$

Then, because the summations for the pressure coefficients (eqs. (14), (16), and (18)) contain the surface shape factor $h(x)$ (expressed in a Fourier series), the pressure distributions calculated for the single mean sine wave are corrected back to the original wave shape by multiplying the coefficients by the shape-ratio parameter

$$\frac{h(x)}{h_m \sin\left(n\pi \frac{x}{l}\right)} \tag{23}$$

Equations (14), (16), and (18) are thus converted into the following simpler forms:

For the basic case,

$$C_p(x, r_m) = -\frac{2\pi}{\beta}\frac{h(x)}{l}\frac{K_0\left(\beta\pi\frac{r_m}{l}\right)}{K_1\left(\beta\pi\frac{r_m}{l}\right)} \tag{24}$$

for the slender cylinder case,

$$C_p(x, r_m) \approx -2\pi^2\frac{r_m}{l^2}h(x)\log_e\left(\beta\pi\frac{r_m}{l}\right) \tag{25}$$

and for the two-dimensional case,

$$C_p(x) \approx -\frac{2\pi}{\beta}\frac{h(x)}{l} \tag{26}$$

In essence, equations (24) to (26) specify that, to a first order, the shapes of the pressure distributions over arbitrarily shaped, periodic transverse waves will match the shapes of the waves themselves except for a multiplicative constant. A comparison of the simplified or approximate theory with exact theory for a range of wave shapes is required to establish the usefulness of the proposed simplification.

COMPARISON WITH EXPERIMENT

Experimental results of finite wavy surfaces are available in reference 4. Photographs of typical roughness models used in that investigation are shown in figure 3. A comparison of the theory with the subsonic experimental results of reference 4 is presented in figures 4 to 12. For reasons which will be discussed in the next section the comparison of the basic theory has been limited to one test Mach number (0.70) and to three experimental configurations, one of which is such a shape (the model with steps normal to the free-stream flow, fig. 4) that the theory should not apply. The comparison of the simplified or approximate theory, however, covers the six roughness configurations and two available subsonic test Mach numbers (0.70 and 0.90). In order to shorten the calculations, the assumption was made throughout the analysis that free-stream flow conditions existed at the roughness elements. The theoretical increments in pressure distribution were added to the experimental smooth-model reference pressure distribution for the comparison. This procedure eliminates the possibility that problems concerned with the calculation of the theoretical pressure distributions over the smooth

reference ogive cylinder will interfere with the evaluation of the usefulness and accuracy of the theory in determining incremental surface-roughness pressures. Note that in figures 4 to 12 the vertical scale for the surface profiles has been expanded by a factor of approximately 25 relative to the horizontal scale (in true relative physical scales) to show adequately the detailed features of the roughness elements.

An inspection of figures 4 to 12 reveals a wide variety of agreement or disagreement between theory and experiment. This multiplicity of agreements can be explained only by detailed consideration of all possible sources of violations of the assumptions and problems inherent in the theory. In the order that they are discussed, these considerations are:

Computation problem for basic theory
Use of the approximate theory
Variations in model cylinder mean radius
Nonuniform local flow conditions
Nonuniform roughness-cycle repetition
Violation of criterion $\left|\frac{dh}{dx}\right| \ll 1$
Violation of criterion $\left|\frac{d^2h}{dx^2}\right| \ll 1$
Boundary-layer effects
Finite number of experimental roughness cycles
Neglect of roughness sweepback

Computation Problem for Basic Theory

One of the notable features of the comparison of the basic theory with experiment in figures 4 to 6 is the rather jagged theoretical pressure distributions. This jaggedness, which tends to be somewhat obscured in the region of sharp pressure changes, remains about the same order of magnitude whether 6, 10, 20, or 29 Fourier terms were used in the pressure computations. Calculations confirmed that the same problem existed for an idealized smooth-surface step configuration. The problem, hence, is not associated with the relative smoothness of the roughness configurations but is connected with the fact that the pressure coefficients are obtained by differentiating a Fourier series (see eqs. (12) and (13)), and differentiated Fourier series are notoriously slow in convergence or do not converge at all (ref. 10). Specifically, the predicament arises because the basic roughness surface (even if perfectly smooth on a small scale) is represented by a continuous but undulating curve which may represent the surface height distribution with reasonable accuracy, but the local slopes of the undulating curve generally do not match those of the basic surface with sufficient accuracy. Although an increase in the number of terms in the series will improve the representation of the basic surface,

the shortened intervals for the higher terms tend to counterbalance most of the desired improvements in the local shape. This problem, of course, tends to limit the usefulness of the basic theory. Several procedures can be devised to overcome this deficiency, but, inasmuch as they require some development and fairly extensive checking, they were considered to be outside the scope of the present investigation.

Use of the Approximate Theory

The major effects of using the approximate or simplified theory were to eliminate the jaggedness in the theoretical curves and, at the same time, to lose effectiveness in prediction of the pressures for models approaching a rectangular roughness shape. (Compare figs. 4, 5, and 6 with figs. 7, 8, and 9, respectively.) For the stepped roughness configuration (figs. 4 and 7), for example, there was a loss in effectiveness of predicting the shape of the pressure distribution because the basic pressure distribution was replaced by an essentially constant pressure increment which is the mean of the basic pressure increments. An analysis indicates that this deterioration begins as the shape of the roughness elements departs from that of a simple sine (or cosine) wave and increases progressively as the stepped-model shape is approached. The effect is due to the reduced weighting factors used for the higher order terms in the simplified theory and the fact that these higher order terms contribute heavily in the neighborhood of sharp corners. Apparently, this effect is discernible but not serious for the model with 1.35-mm transverse creases. (Compare fig. 6 with fig. 9(a).) Nevertheless, this deterioration is not desirable for accurate work and substantiates the need for improving the basic theory.

Variations in Model Cylinder Mean Radius

The experimental models were not designed with a common mean radius for the cylindrical portions of the models. For example, the model with the 1.35-mm protruding waves was designed with all parts of the roughness elements lying everywhere above the mean radius of the smooth reference model (53.0 mm), whereas the model with the 1.35-mm transverse creases was designed with all parts of the waves lying everywhere beneath the reference mean radius. Because the radius of the end of the nose ogive was held approximately constant for all models, there was an increase in the mean radius of the cylinder with reference to the ogive radius for the first model and a decrease for the second. As a consequence, the correct smooth-body reference pressures for some of the models differ somewhat from the single reference pressure distribution that is used herein. This discrepancy can be divided into two parts. The first and probably most significant discrepancy occurs just behind the ogive-cylinder juncture and decreases rapidly with distance downstream. The second discrepancy, which derives from the recompression of the flow from different base areas, is greatest at the trailing edge of the

models and decreases rapidly with distance upstream. The discrepancies theoretically may be observable under highly accurate conditions, but attempts to identify their existence were not successful. The discrepancies, hence, are believed to be relatively small and the effects on the agreement between theory and experiment are consequently believed to be generally negligible for the measurement stations of this investigation.

Nonuniform Local Flow Conditions

The theory, of course, is predicated upon a constant free-stream velocity. Because the local velocities on the smooth reference body vary slightly over the length of the cylinder (see fig. 5 of ref. 4), this requirement was met only approximately. Furthermore, in order to simplify the theoretical calculations, they were made with the assumption that the mean local velocity was equal to the free-stream velocity. Check calculations indicated that the errors due to the last assumption were not significant. An approximate evaluation of the effects of the nonuniform local flow velocities indicated that the effects were somewhat larger than those due to the assumption of free-stream mean velocity but still of no great importance within the context of the present analysis. In most practical situations, however, neither one of the problems would disappear so readily and could significantly influence the agreement between theory and experiment.

Nonuniform Roughness-Cycle Repetition

The effects of nonuniform cycle repetition (compare shapes of forward and rearward measurement stations in figs. 7 to 12) cannot be calculated directly. Theoretical indications are nevertheless that the effects of a roughness element on the pressure distribution on another roughness element will decrease rapidly with distance between the two elements. Furthermore, the deviations in the shapes of the many individual roughness elements are random in nature and thus will cancel, on the average, the effects of each other on any specified element. Consequently, the overall effect of a multitude of roughness elements of slightly different shape on any individual element is very small and probably negligible. This indication is amply supported by the experimental results (figs. 7 to 12), which show a wide variation in pressure distribution shapes between the forward and rearward roughness elements and a strong tendency for the distributions to follow the shape of the local roughness element except in the neighborhood of corners. This tendency was incorporated into both the basic and approximate theories. In the basic theory, the incorporation was accomplished by calculating the pressure distribution for the forward element with the assumption that the shape of the forward roughness element was the mean for all the elements and calculating the pressure distribution for the rearward element with the assumption that the shape of the rearward element was the mean for all the elements. In the approximate theory, the tendency was specified as a

direct requirement (excessively, in the case of the step-type roughness models) in equations (24) to (26). Without the incorporation of the tendency into the theories, the agreement between theory and experiment will deteriorate.

Violation of Criterion $\left|\frac{dh}{dx}\right| << 1$

Past experience at low subsonic speeds indicates that nonlinear effects are usually negligible and the possibility of flow separation with turbulent boundary layer is generally remote if the local surface angle relative to the undisturbed free-stream flow is less than $\pm 10^{\circ}$ $\left(\left|\frac{dh}{dx}\right| << 0.18\right)$. (See ref. 11, for example.) This criterion is met generously everywhere except on the vertical faces of the stepped roughness configurations (figs. 4, 7, and 11) and in limited areas of the creases at station 1 on the model with 1.35-mm transverse creases (figs. 6 and 9). The vertical step faces are actually immersed in a separated flow which reduces the angle of the flow just outside this region to a considerably lower value than that of the step face. This exterior flow has a much stronger influence on the neighboring pressure distributions than that of the separation vortex itself. If the shape of the separation streamline were known, the effects of flow separation could be incorporated into the basic theory and would improve the calculation of pressure distribution close to square corners. Obviously, except for regions close to the step faces and possibly some crease areas, there should be no deterioration in the theoretical calculations due to excessive local surface slopes or the violation of the criterion $\left|\frac{dh}{dx}\right| << 1$

Violation of Criterion $\left|\frac{d^2h}{dx^2}\right| << 1$

The criterion that $\left|\frac{d^2h}{dx^2}\right| << 1$ can be shown to enter the problem in approximately the same fashion as the slope parameter itself, but the empirical limiting values are not nearly as well established. Violations of this criterion occur at the corners of the steps (figs. 4, 7, and 11) and in the creases of the three creased models (figs. 6, 9, 10, and 12). The effects tend to die out rapidly with distance from the source of the violation and the effects are believed to be relatively small and highly localized although probably discernible in the experimental results. If the flow separation at the corners is accounted for, the theoretical magnitude of this effect will be sharply reduced. As for the slope parameter, significant deterioration in the theoretical calculations should be limited to the region neighboring step faces and creases.

Boundary-Layer Effects

Boundary-layer effects are not incorporated into the theory and must be inferred from a comparison of experiment with theory and changes in experimental pressure distributions with change in test unit Reynolds number. In general, the experimental effects of changes in unit Reynolds number were greatest for the highest roughness elements and least for the lowest ones. (See figs. 7 to 12.) For the lowest roughness elements, the changes were often within experimental error. The data also appear to indicate a tendency toward smaller changes at the higher Reynolds numbers, as though the boundary-layer effects were disappearing at the high values of unit Reynolds number. A comparison of theory and experiment indicates that the discrepancy is largest at the rearward measurement station where the ratio of roughness height to boundary-layer thickness is least.

An analysis of these trends suggests that there are two essentially different boundary-layer effects. One effect is related to the roughness-height—boundary-layer-thickness ratio. The lower this ratio the less the theoretical compressibility effects are allowed to develop because the local velocities close to the roughness surface are smaller than those indicated by the inviscid theory. The second effect is related to the boundary-layer displacement-thickness effects superimposed on the basic roughness-element contours. In effect, the roughness height is decreased and even the $M_\infty = 0$ pressure distribution cannot be attained. The two boundary-layer effects just discussed probably account for most of the discrepancy between theory and experiment for the unswept roughness configurations except for regions close to sharp corners on those models having them.

Finite Number of Experimental Roughness Cycles

Because the effects of those portions of a roughness element that protrude above the mean cylinder radius will, at a distance, cancel approximately those effects induced by the portions of the element lying below the mean radius, the effects of one roughness cycle on any other roughness cycle should be small. Also, for elements located approximately centrally in a group, the residual uncanceled effects from the upstream elements will tend to cancel those from the downstream elements. Without a more extensive analysis, however, one cannot establish that the summation of the residual uncanceled effects will be negligible for those elements lying close to the ends of a finite group. As a result, some allowance must be made for the possibility that part of the disagreement between theory and experiment in this investigation may be due to the finite number of experimental roughness cycles and the measurement of pressure distributions on elements close to the ends of the group.

Neglect of Roughness Sweepback

The theory does not apply to swept roughness configurations. However, inasmuch as the analysis of the results for the unswept configurations (figs. 7 to 10) implies that the pressure distribution over an individual roughness element is primarily determined by the shape characteristics of that element, the possibility arises that the theory can predict the first-order pressure distribution characteristics of swept configurations. A comparison of theory with experiment in figures 11 and 12 appears to confirm this observation. In fact, if the component of the free-stream flow normal to the roughness element were used, the agreement between theory and experiment would be improved somewhat. Boundary-layer effects would still prevent theory from agreeing with experiment.

CONCLUSIONS

The theoretical solution for the pressure distribution over an infinitely repeating set of sinusoidal waves in subsonic, compressible flow is extended to the case of arbitrarily shaped periodic waves by the use of Fourier series, and a simplified or approximate solution for the calculation of first-order effects is developed. The solutions are compared with the experimental pressure distributions of NASA TN D-3516 determined at Mach numbers of 0.70 and 0.90 on six types of roughness elements incorporated into the cylindrical portions of a group of ogive cylinders. The comparisons are discussed in terms of violations of the restrictions and assumptions inherent in the theory. They lead to the following conclusions.

1. The basic theory has an excellent potential for prediction of inviscid roughness pressure distributions over arbitrarily shaped, periodic surface roughness elements but a smoothing procedure must be incorporated to realize the full potential.

2. For estimation of first-order effects, the approximate or simplified theory is quite satisfactory for approximately sinusoidal shapes, but tends to deteriorate in usefulness as a square-cornered, rectangular roughness shape is approached.

3. Agreement of theory with experiment is poor because boundary-layer effects strongly delay the onset of the compressibility effects predicted by the theory and even prevent the incompressible-flow pressure distribution from being realized.

4. Extension of the theory to predict first-order sweep effects may be possible by using an approach which utilizes the component of the free-stream flow normal to the roughness element.

Langley Research Center,
National Aeronautics and Space Administration,
Hampton, Va., July 31, 1970.

REFERENCES

1. Czarnecki, K. R.; and Monta, William J.: Pressure Drags Due to Two-Dimensional Fabrication-Type Surface Roughness on an Ogive Cylinder at Transonic Speeds. NASA TN D-3519, 1966.

2. Czarnecki, K. R.; and Monta, William J.: Roughness Drag Due to Two-Dimensional Fabrication-Type Surface Roughness on an Ogive Cylinder From Force Tests at Transonic Speeds. NASA TN D-5004, 1969.

3. Czarnecki, K. R.; and Monta, William J.: Pressure Distributions and Wave Drag Due to Two-Dimensional Fabrication-Type Surface Roughness on an Ogive Cylinder at Mach Numbers of 1.61 and 2.01. NASA TN D-835, 1961.

4. Czarnecki, K. R.; and Monta, William J.: Pressure Distributions Due to Two-Dimensional Fabrication-Type Surface Roughness on an Ogive Cylinder at Transonic Speeds. NASA TN D-3516, 1966.

5. Margenau, Henry; and Murphy, George Moseley: The Mathematics of Physics and Chemistry. Second ed., D. Van Nostrand Co., Inc., c.1956.

6. Hildebrand, Francis B.: Advanced Calculus for Applications. Prentice-Hall, Inc., c.1962.

7. Sears, W. R., ed.: General Theory of High Speed Aerodynamics. Vol. VI of High Speed Aerodynamics and Jet Propulsion, Princeton Univ. Press, 1954.

8. Reissner, Eric: On Compressibility Corrections for Subsonic Flow Over Bodies of Revolution. NACA TN 1815, 1949.

9. Wylie, C. R., Jr.: Advanced Engineering Mathematics. McGraw-Hill Book Co., Inc., 1951.

10. Sokolnikoff, Ivan S.; and Sokolnikoff, Elizabeth S.: Higher Mathematics for Engineers and Physicists. McGraw-Hill Book Co., Inc., 1934, p. 146.

11. Allen, H. Julian: Calculation of the Chordwise Load Distribution Over Airfoil Sections With Plain, Split, or Serially Hinged Trailing-Edge Flaps. NACA Rep. 634, 1938.

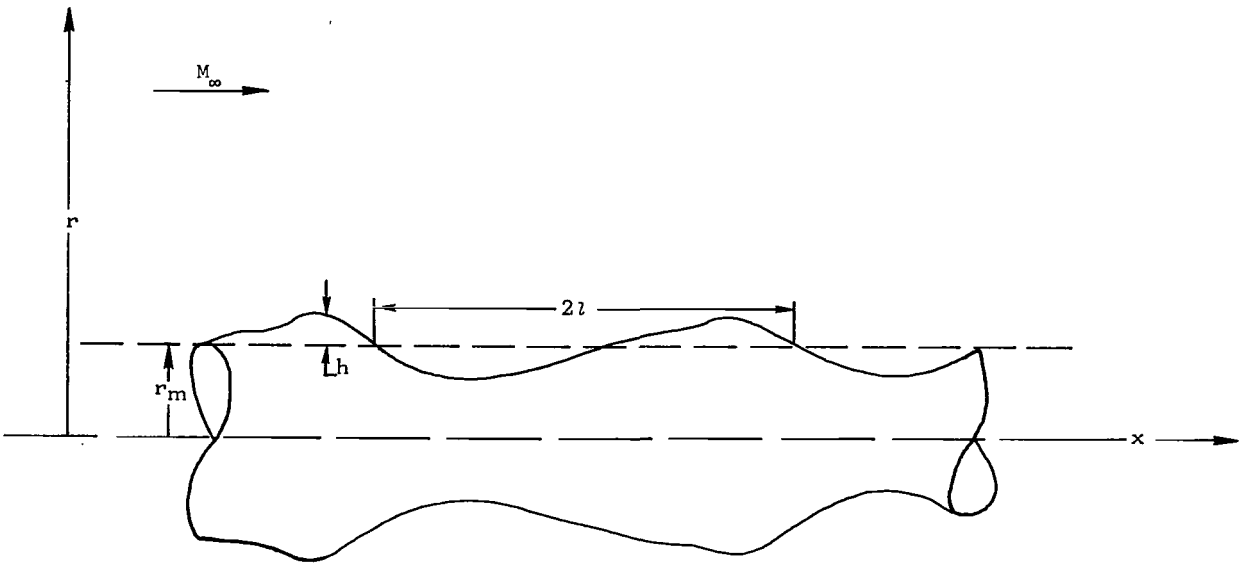

Figure 1.- Infinite cylinder of arbitrarily shaped periodic transverse waves in subsonic axisymmetric flow.

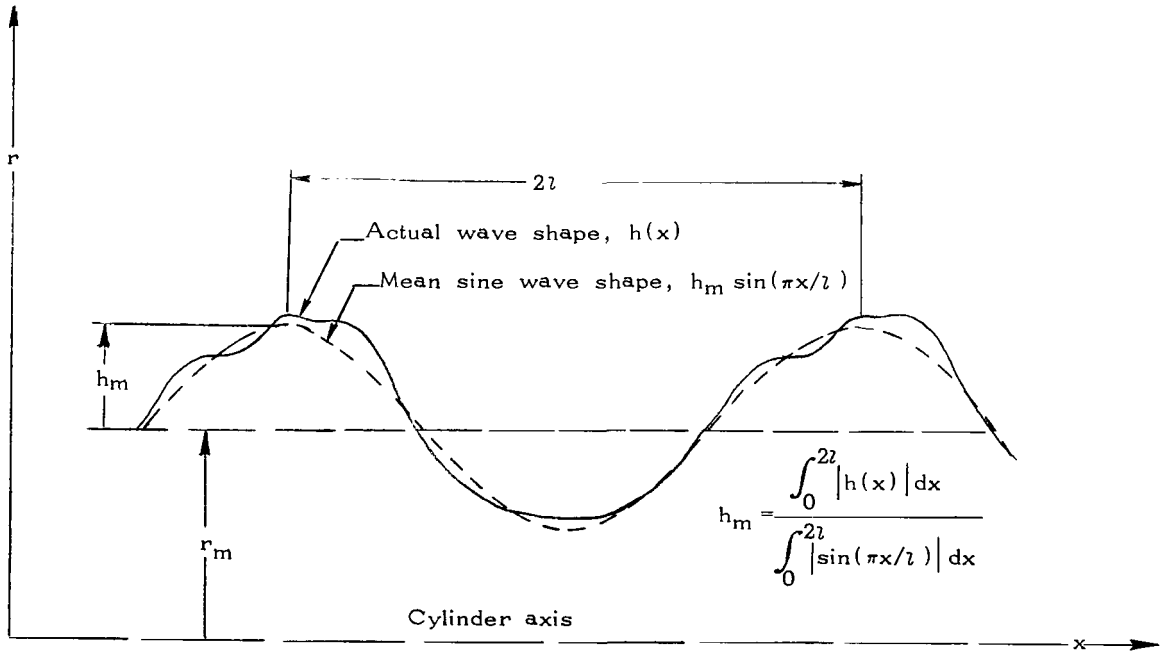

Figure 2.- Relation of mean or fundamental sine wave to actual wave shape.

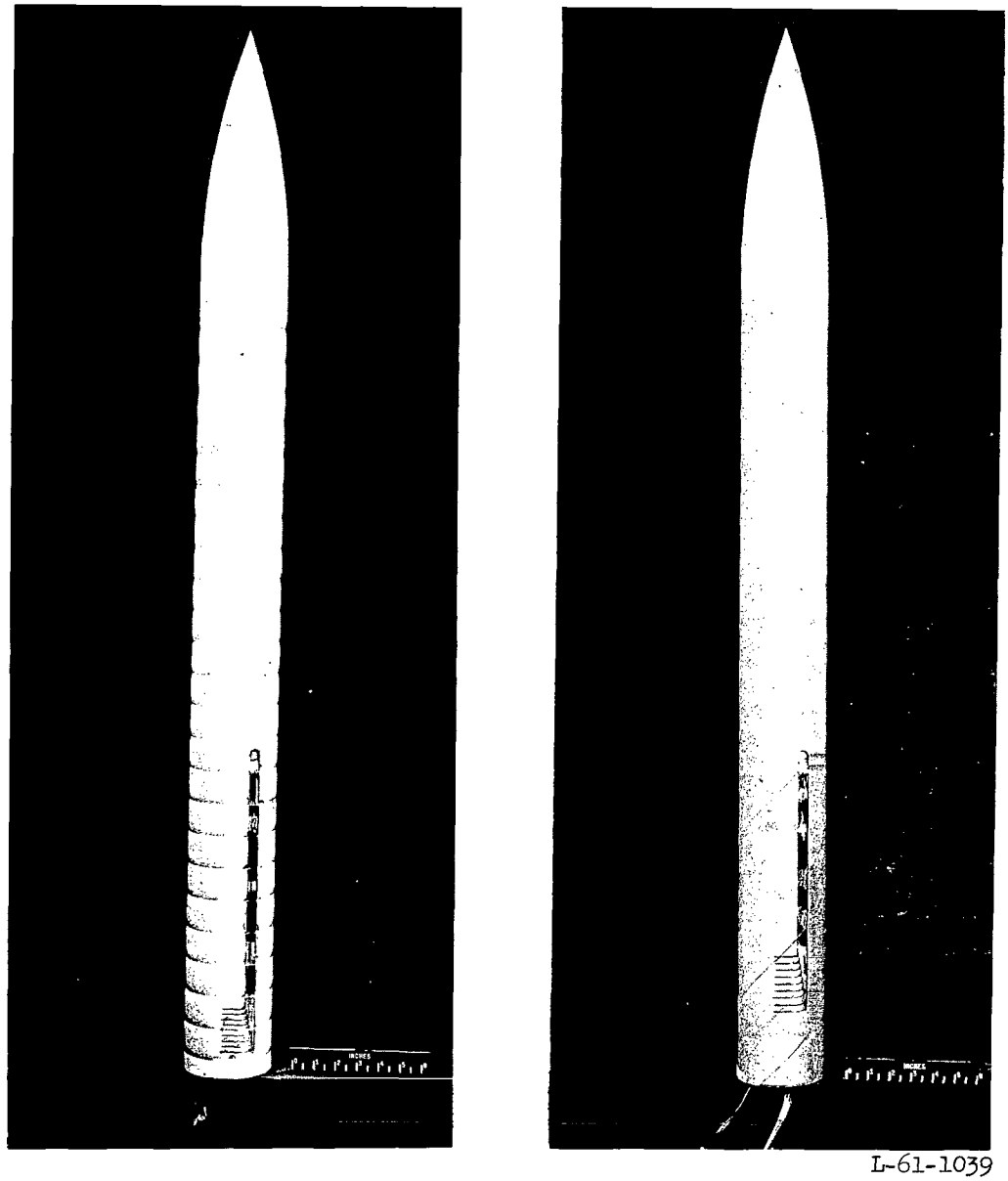

L-61-1039

(a) 1.35-mm transverse creases.

(b) 0.51-mm 45° rearward steps.

Figure 3.- Photographs of typical roughness models (from ref. 4).

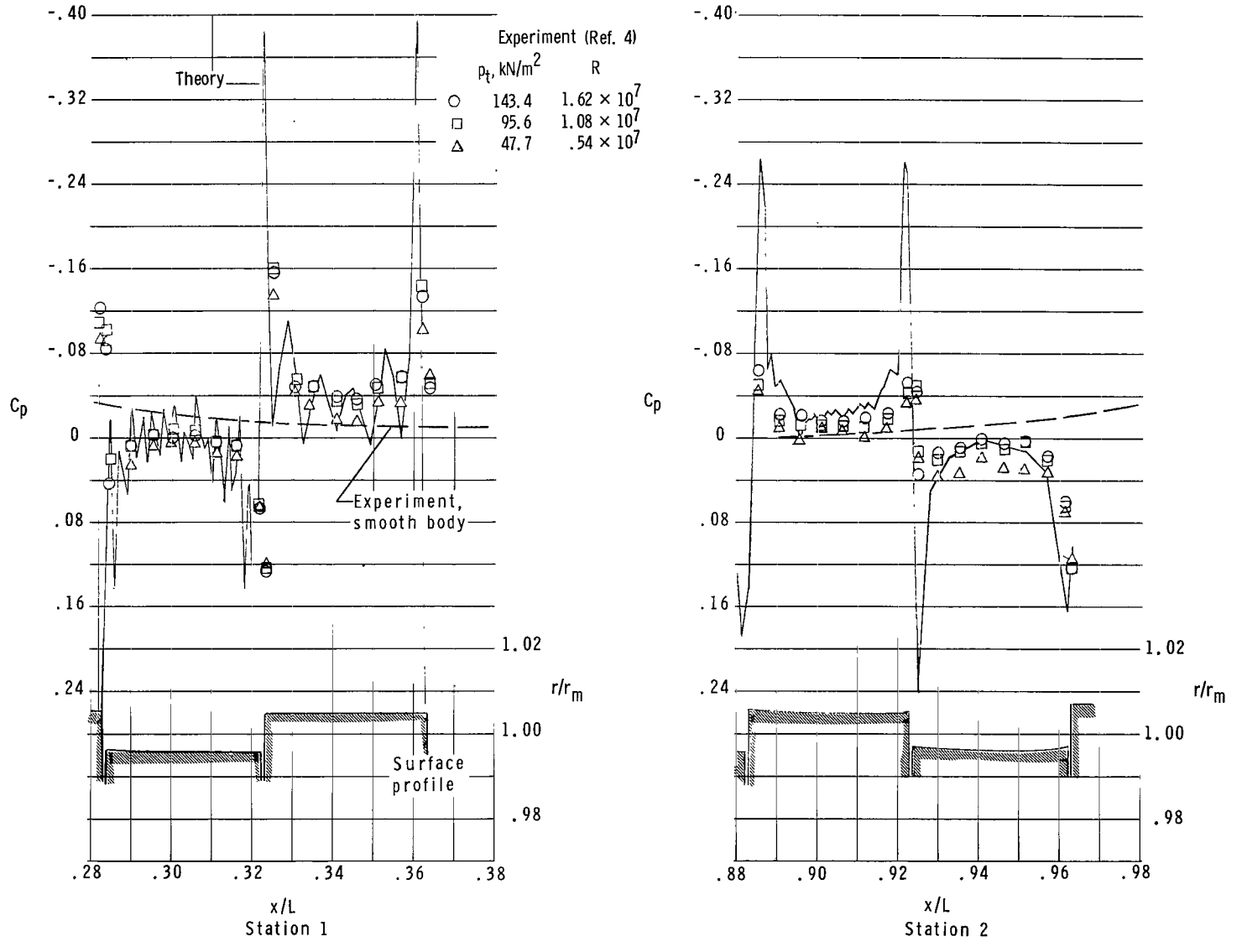

Figure 4.- Comparison of basic theory with experiment. M_∞ = 0.70; model with 0.53-mm steps with grooves.

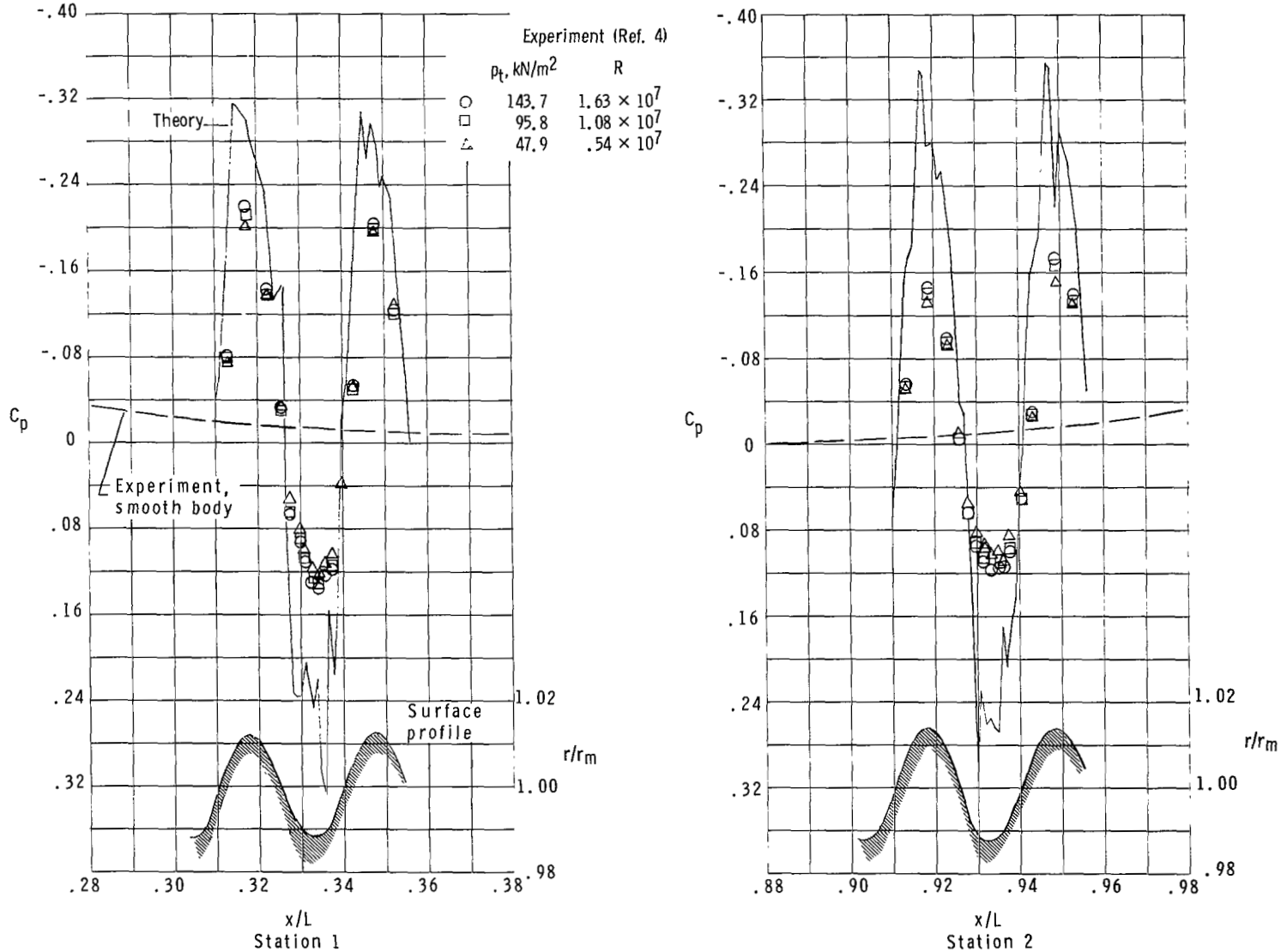

Figure 5.- Comparison of basic theory with experiment. M_∞ = 0.70; model with 1.35-mm protruding waves.

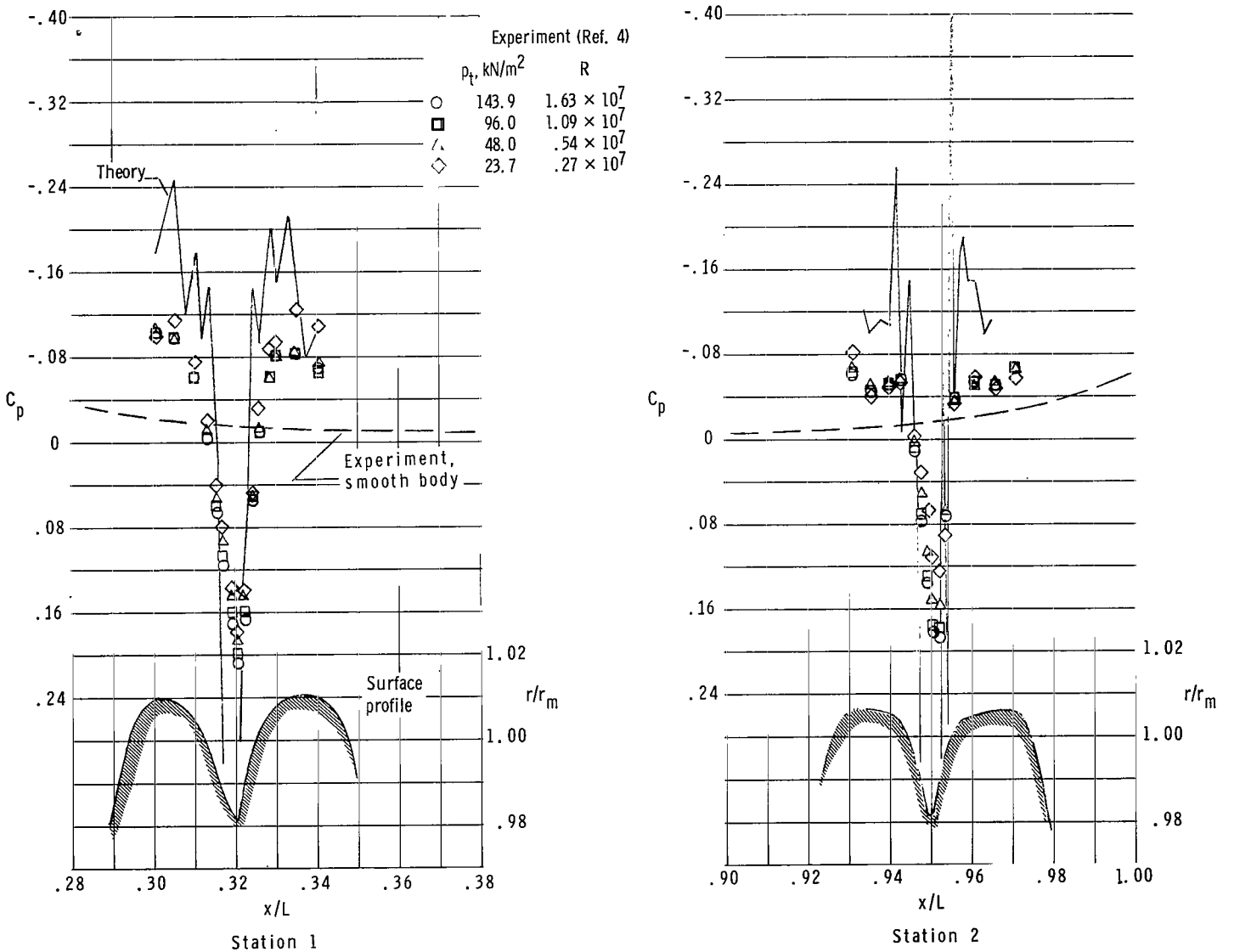

Figure 6.- Comparison of basic theory with experiment. M_∞ = 0.70; model with 1.35-mm transverse creases.

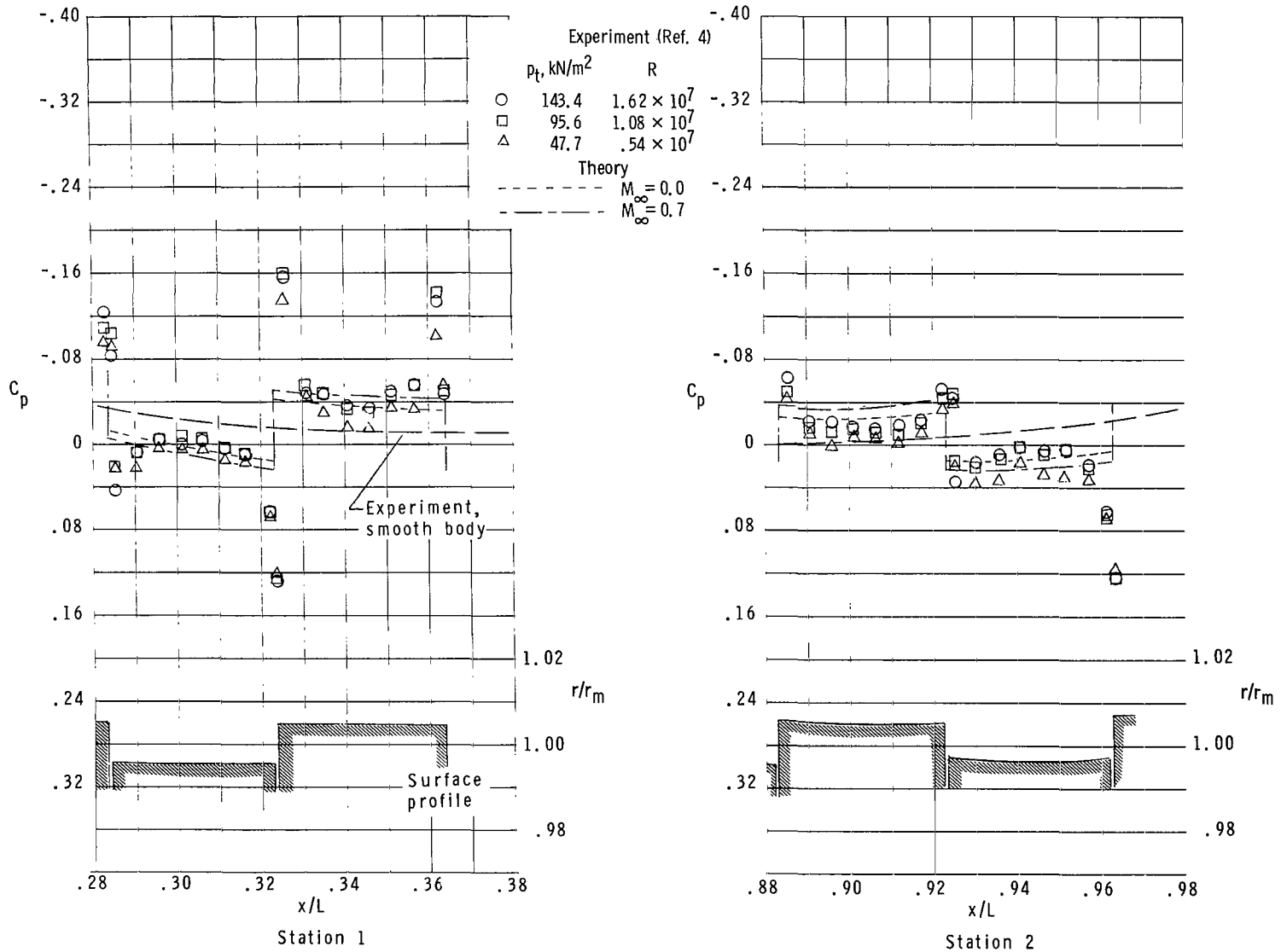

(a) $M_\infty = 0.70$.

Figure 7.- Comparison of approximate theory with experiment. Model with 0.53-mm steps with grooves.

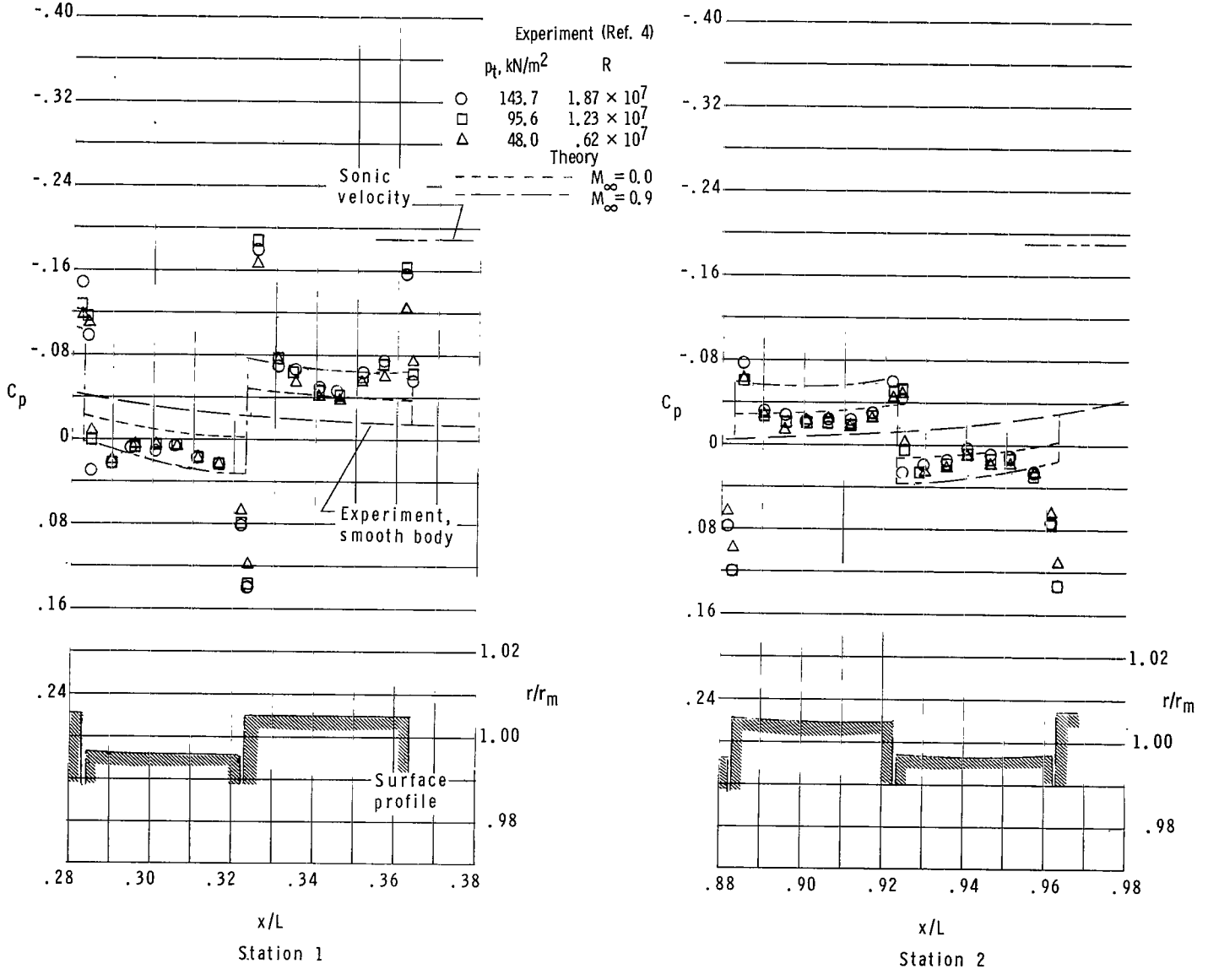

(b) $M_\infty = 0.90$.

Figure 7.- Concluded.

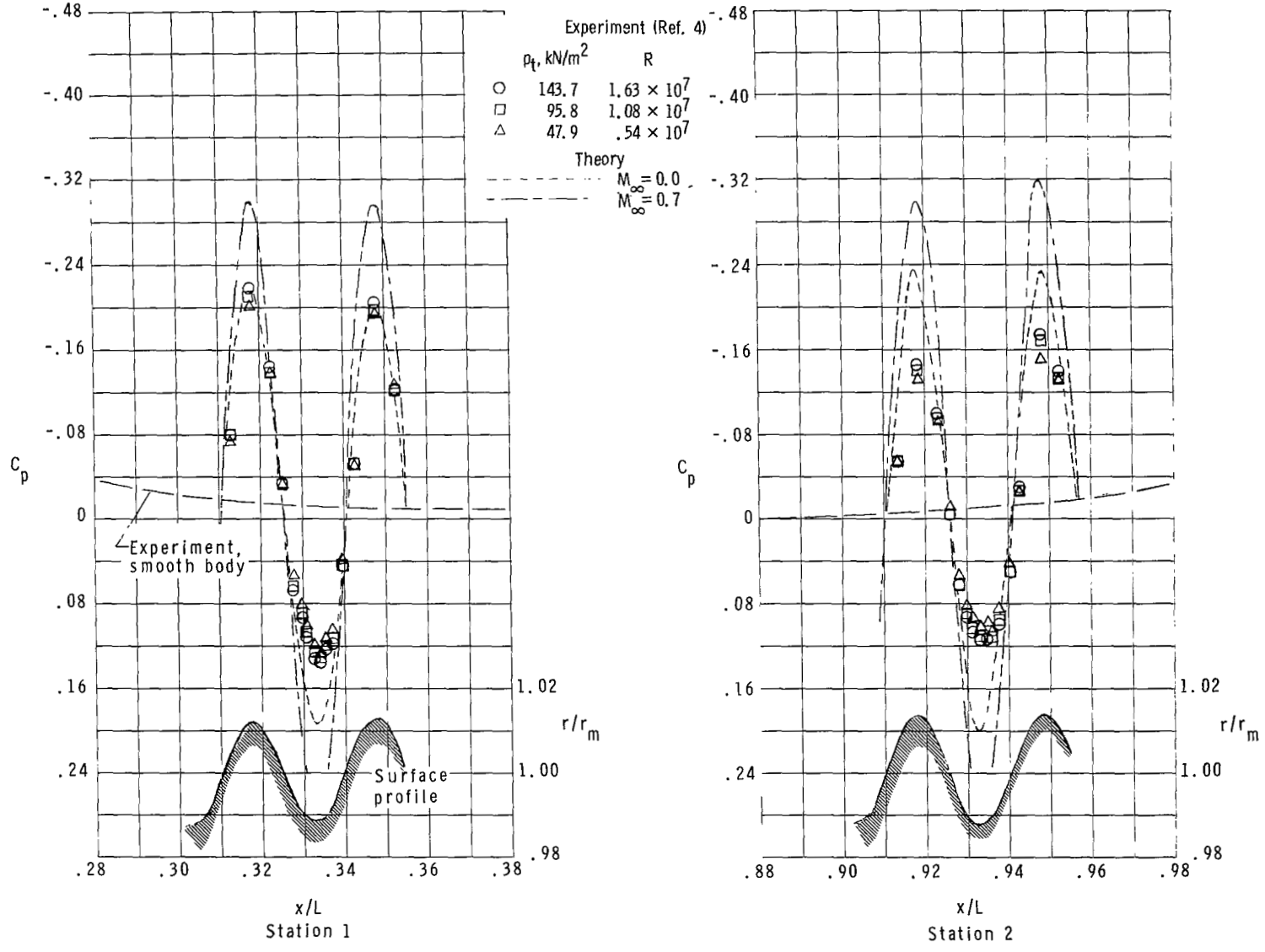

(a) $M_\infty = 0.70$.

Figure 8.- Comparison of approximate theory with experiment. Model with 1.35-mm protruding waves.

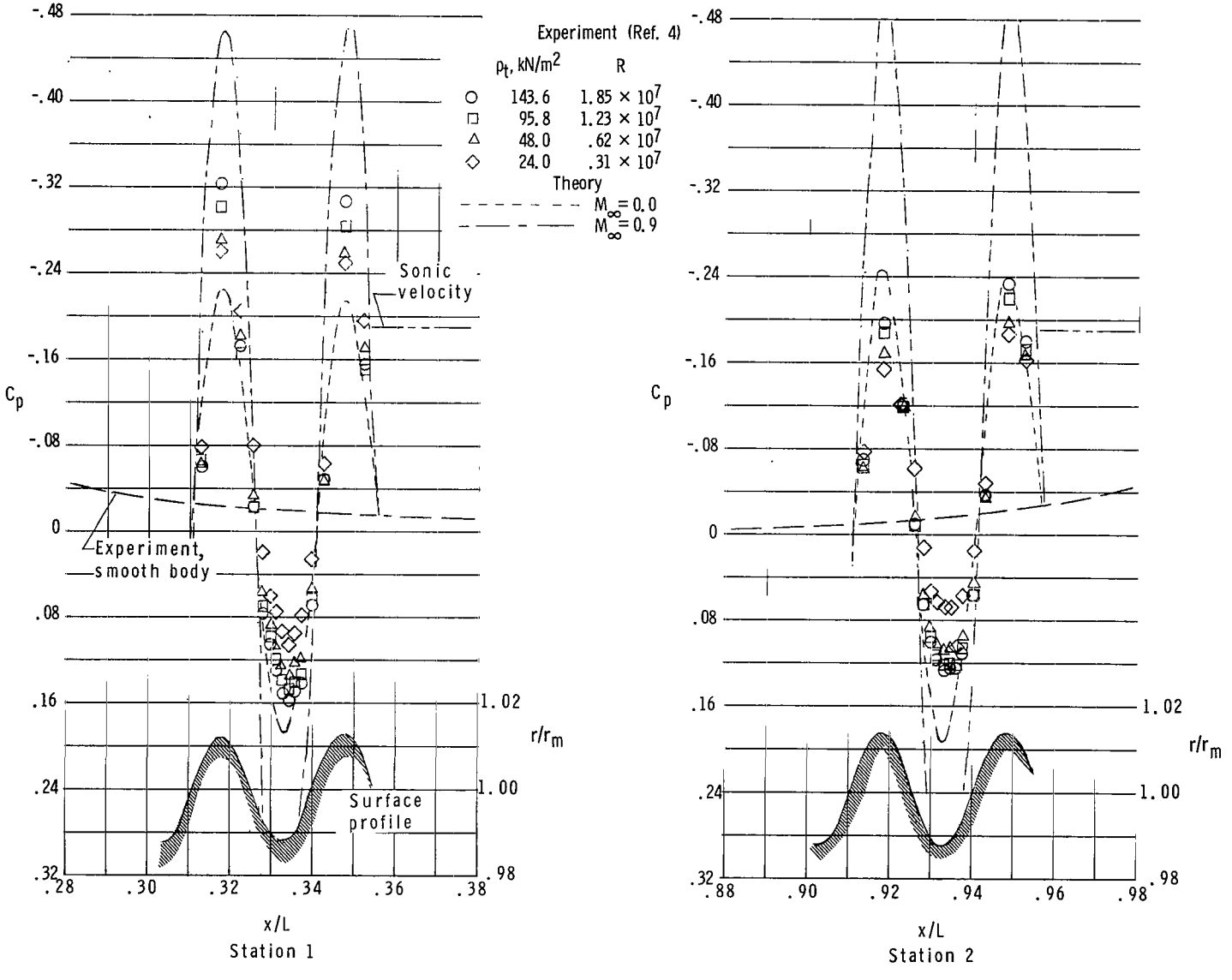

(b) $M_\infty = 0.90$.

Figure 8.- Concluded.

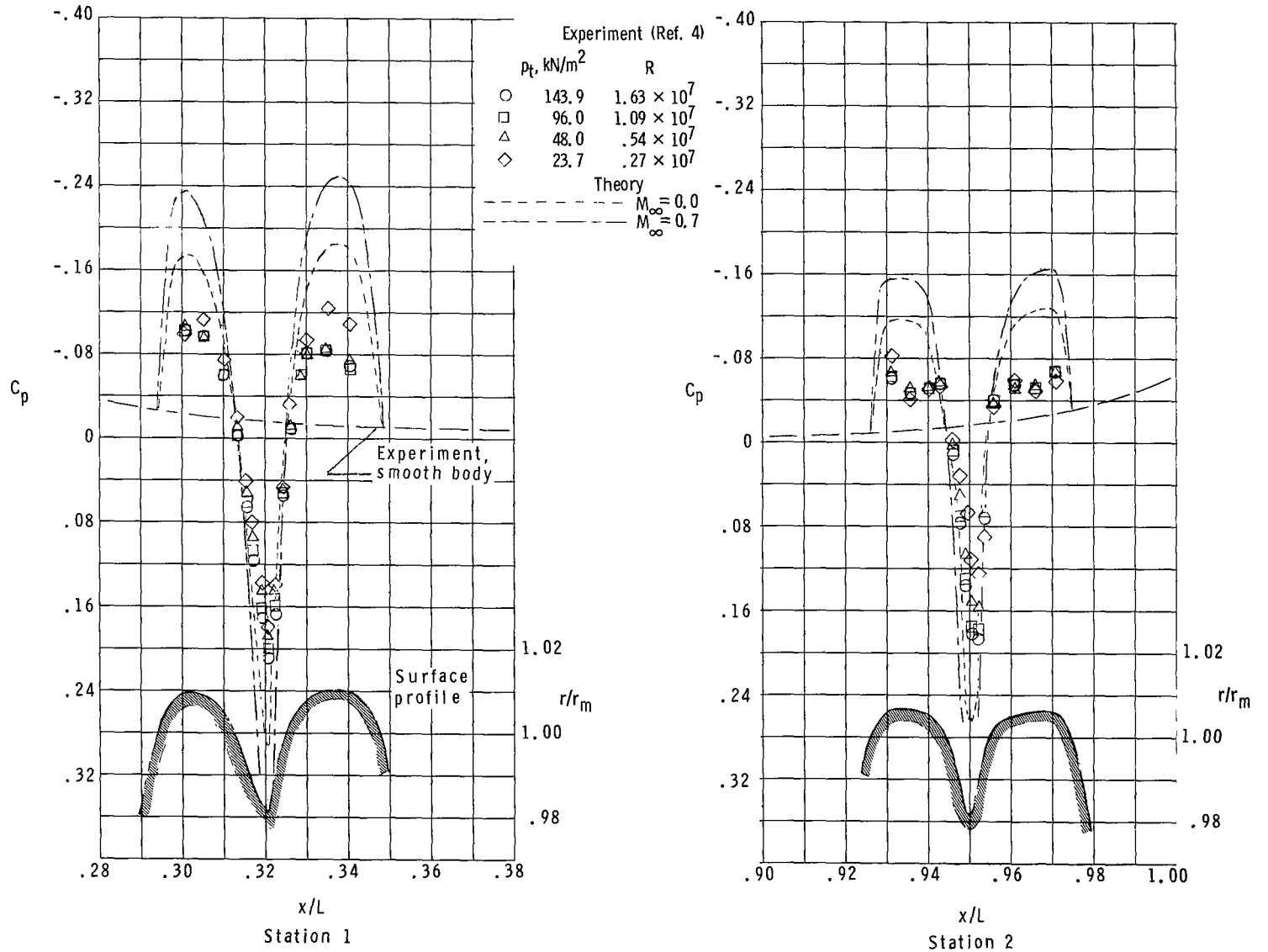

(a) $M_\infty = 0.70$.

Figure 9.- Comparison of approximate theory with experiment. Model with 1.35-mm transverse creases.

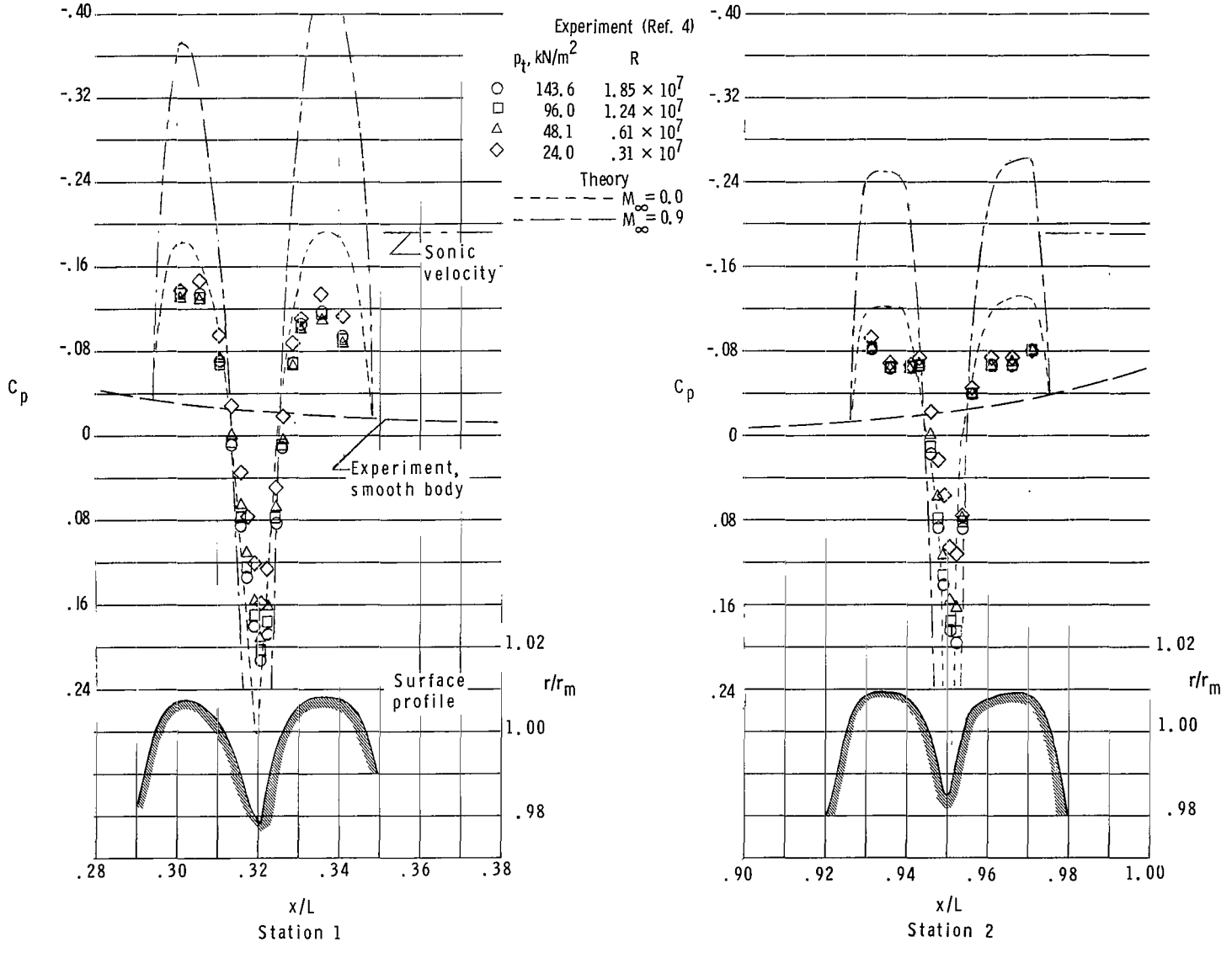

(b) $M_\infty = 0.90$.

Figure 9.- Concluded.

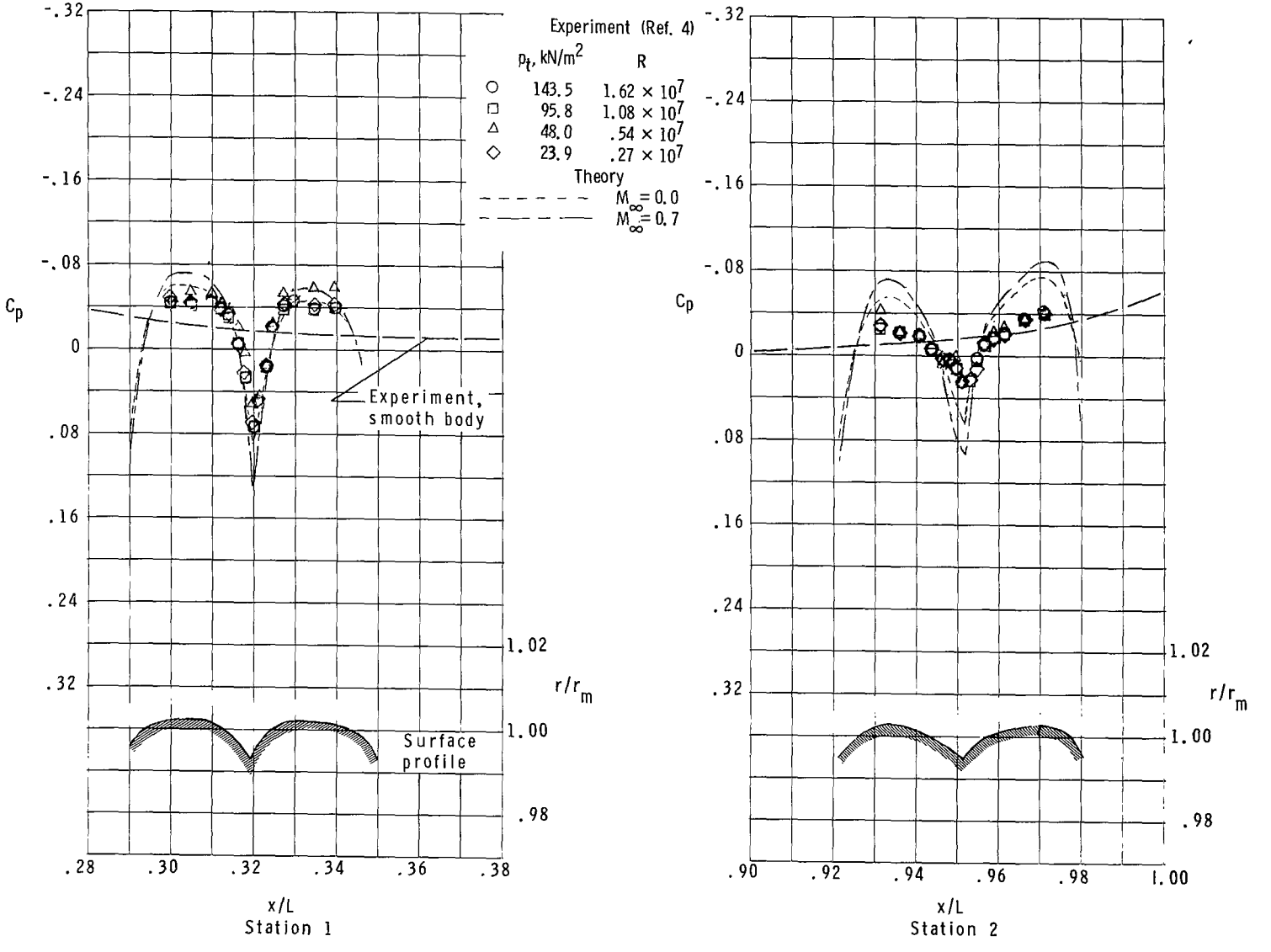

(a) M_∞ = 0.70.

Figure 10.- Comparison of approximate theory with experiment. Model with 0.43-mm transverse creases.

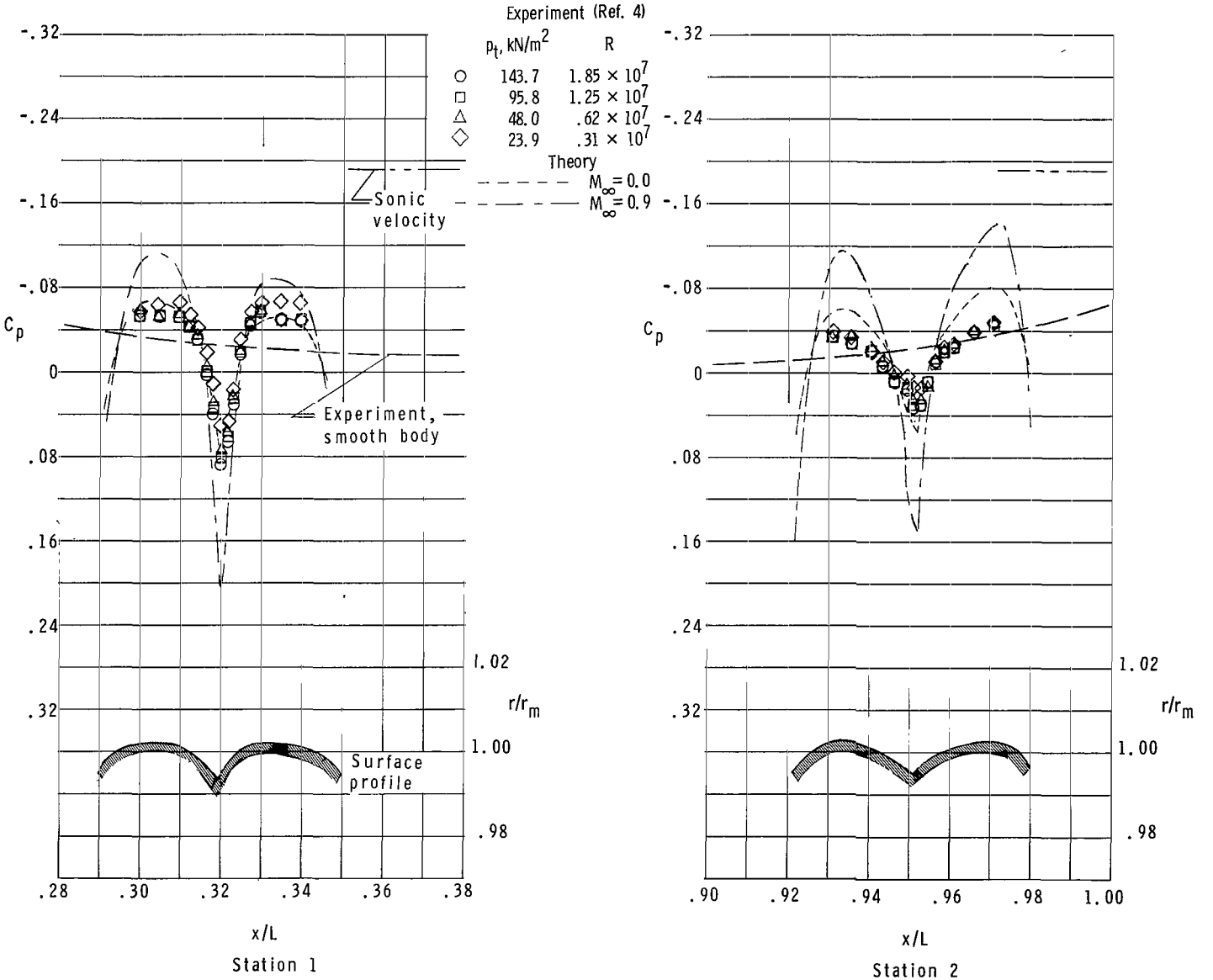

(b) $M_\infty = 0.90$.

Figure 10.- Concluded.

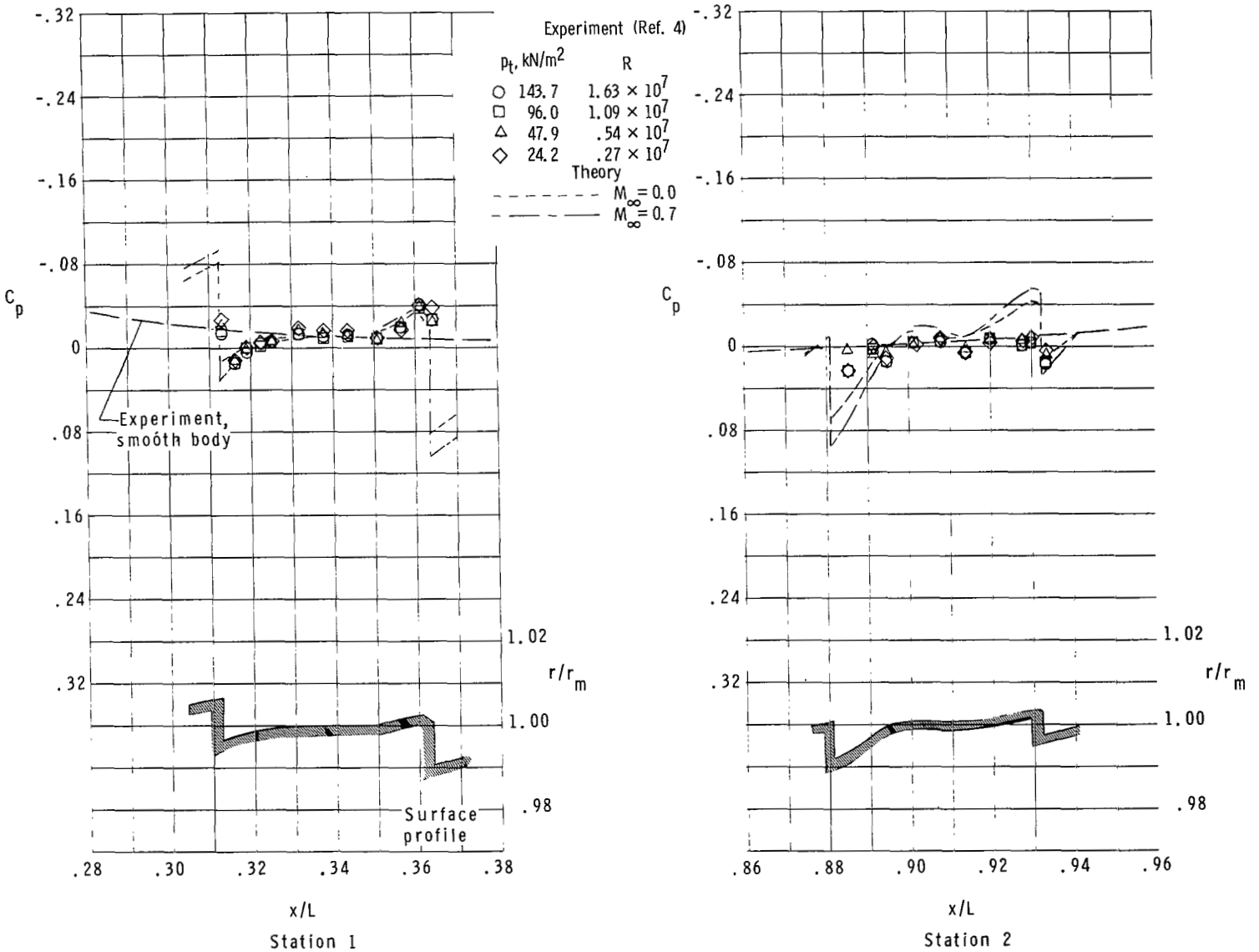

(a) $M_\infty = 0.70$.

Figure 11.- Comparison of approximate theory with experiment. Model with 0.51-mm 45° rearward steps.

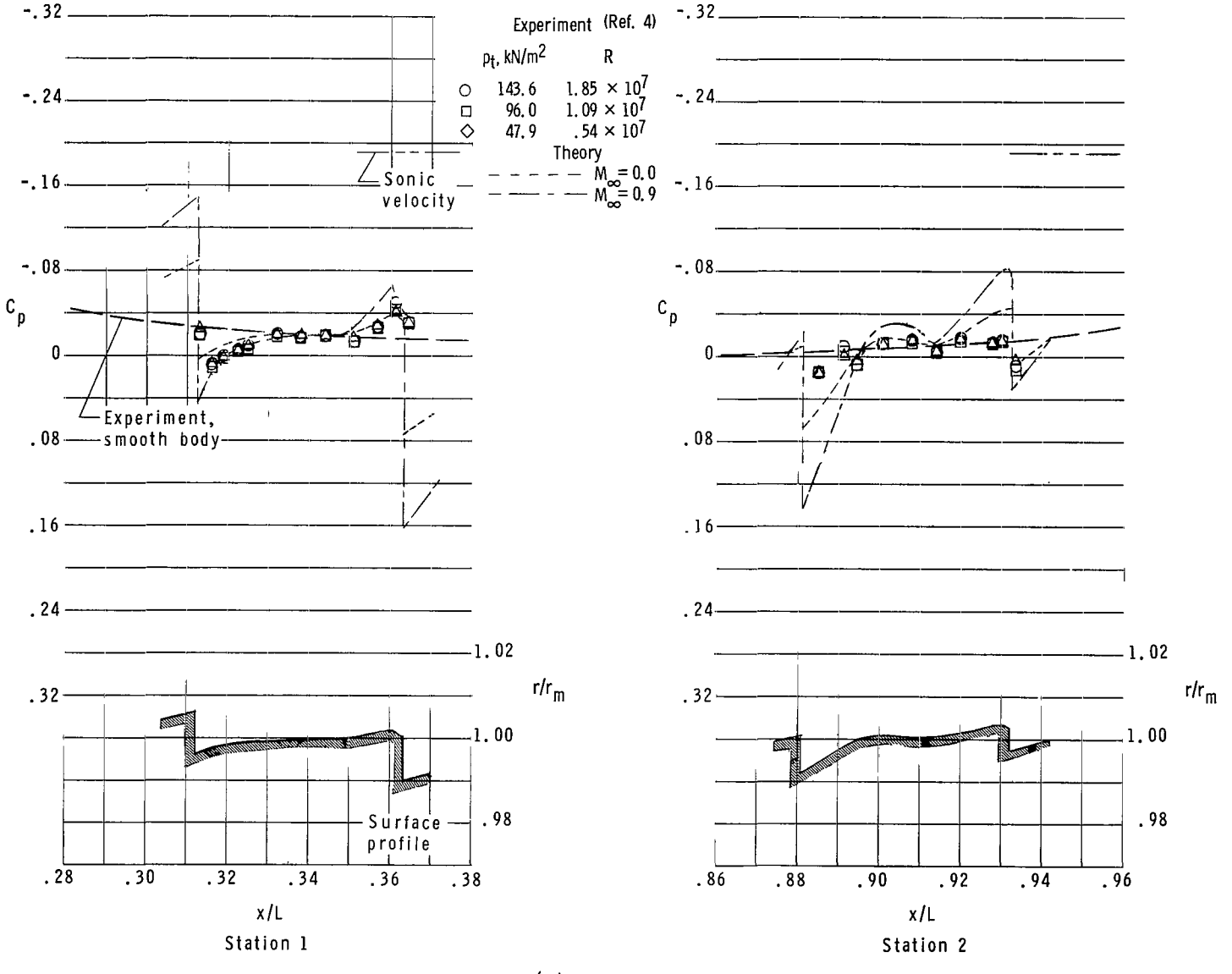

(b) M_∞ = 0.90.

Figure 11.- Concluded.

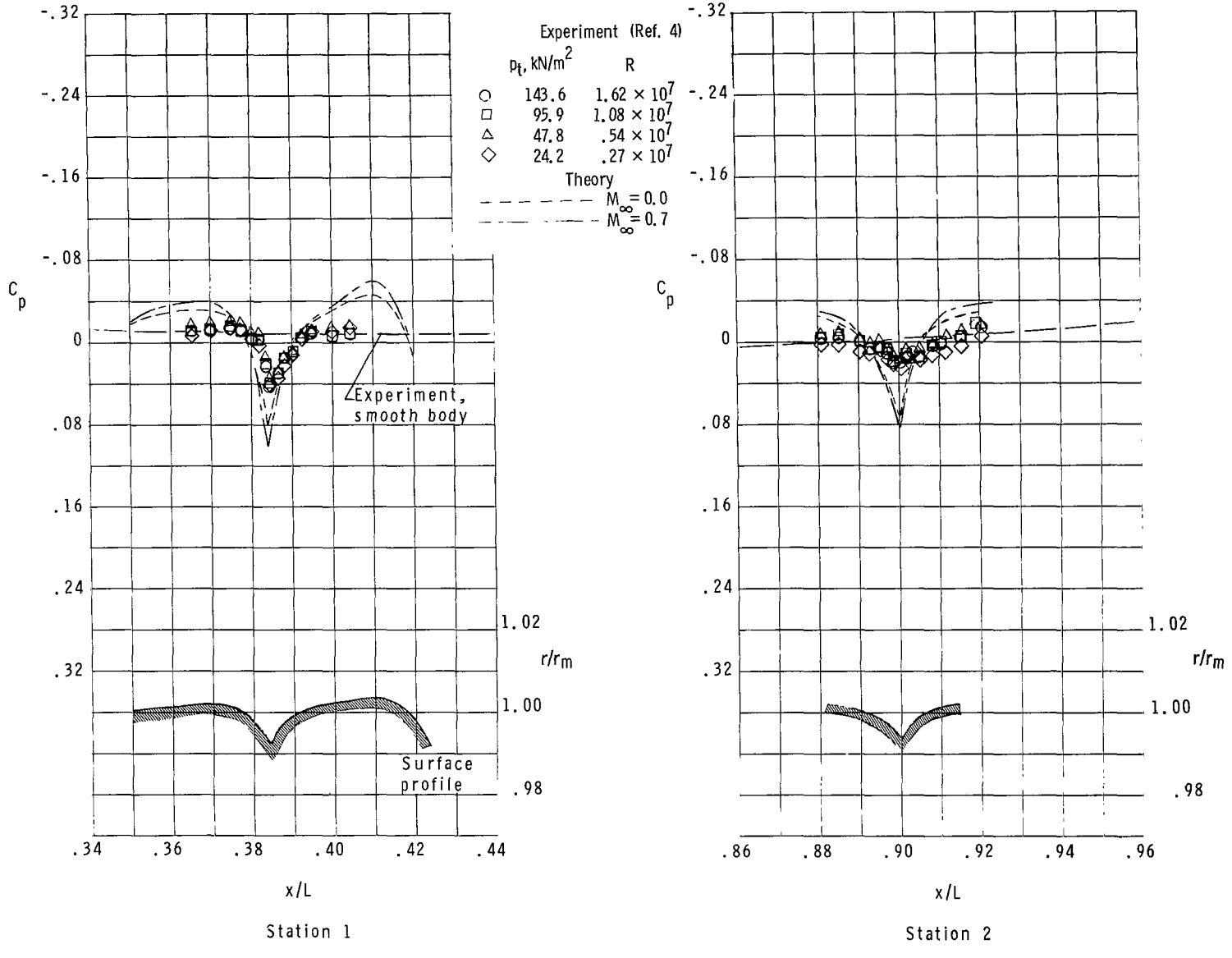

(a) $M_\infty = 0.70$.

Figure 12.- Comparison of approximate theory with experiment. Model with 0.36-mm 45° creases.

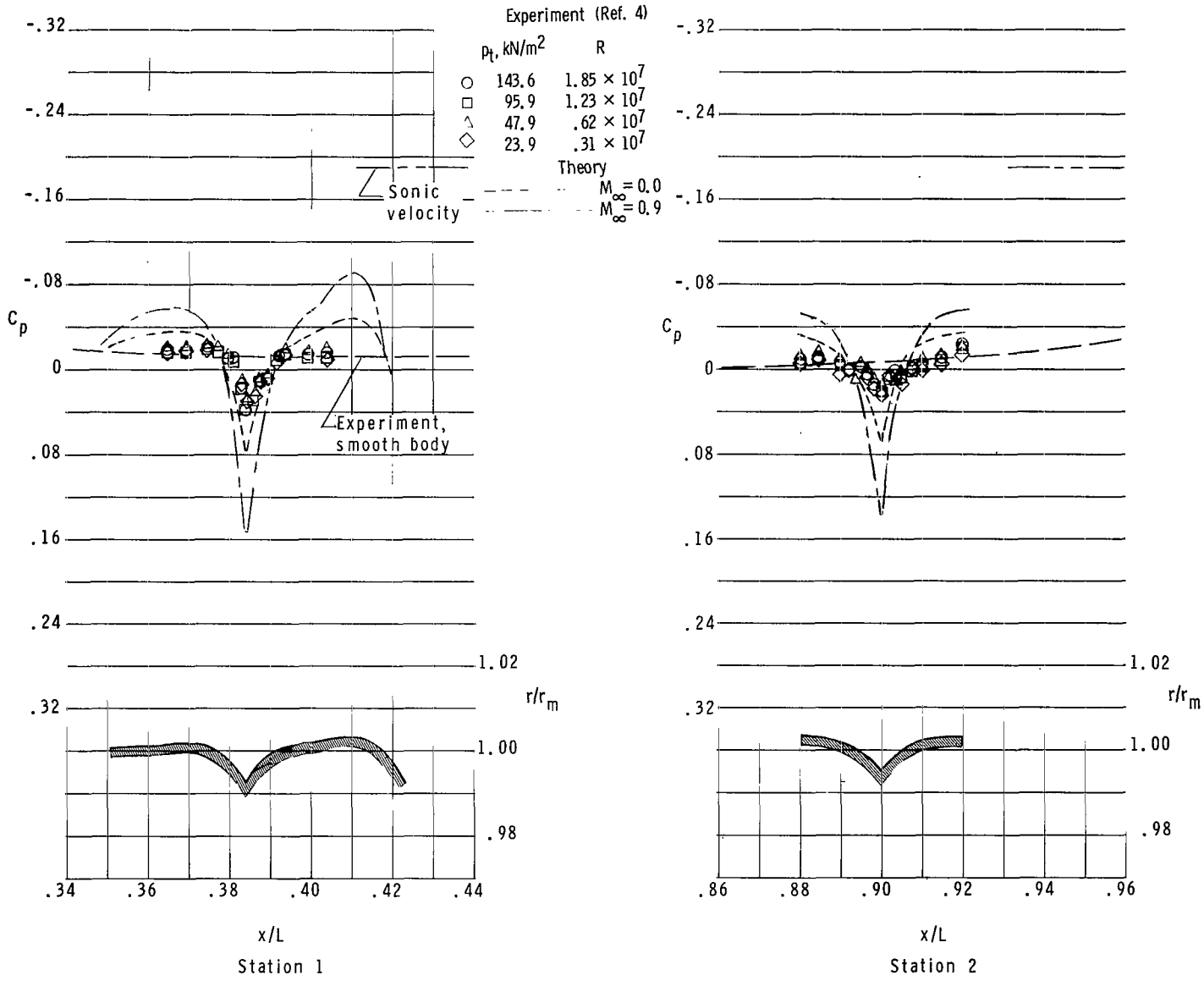

(b) $M_\infty = 0.90$.

Figure 12.- Concluded.

"The aeronautical and space activities of the United States shall be conducted so as to contribute . . . to the expansion of human knowledge of phenomena in the atmosphere and space. The Administration shall provide for the widest practicable and appropriate dissemination of information concerning its activities and the results thereof."

—NATIONAL AERONAUTICS AND SPACE ACT OF 1958

NASA SCIENTIFIC AND TECHNICAL PUBLICATIONS

TECHNICAL REPORTS: Scientific and technical information considered important, complete, and a lasting contribution to existing knowledge.

TECHNICAL NOTES: Information less broad in scope but nevertheless of importance as a contribution to existing knowledge.

TECHNICAL MEMORANDUMS: Information receiving limited distribution because of preliminary data, security classification, or other reasons.

CONTRACTOR REPORTS: Scientific and technical information generated under a NASA contract or grant and considered an important contribution to existing knowledge.

TECHNICAL TRANSLATIONS: Information published in a foreign language considered to merit NASA distribution in English.

SPECIAL PUBLICATIONS: Information derived from or of value to NASA activities. Publications include conference proceedings, monographs, data compilations, handbooks, sourcebooks, and special bibliographies.

TECHNOLOGY UTILIZATION PUBLICATIONS: Information on technology used by NASA that may be of particular interest in commercial and other non-aerospace applications. Publications include Tech Briefs, Technology Utilization Reports and Notes, and Technology Surveys.

Details on the availability of these publications may be obtained from:

SCIENTIFIC AND TECHNICAL INFORMATION DIVISION

NATIONAL AERONAUTICS AND SPACE ADMINISTRATION

Washington, D.C. 20546